The Journal of Chemical Physics

# Quasielastic neutron scattering studies on couplings of protein and water dynamics in hydrated elastin

Cite as: J. Chem. Phys. **152**, 245101 (2020); https://doi.org/10.1063/5.0011107
Submitted: 17 April 2020 . Accepted: 03 June 2020 . Published Online: 30 June 2020

Kerstin Kämpf, Dominik Demuth, Michaela Zamponi, Joachim Wuttke, and Michael Vogel



The Journal of Chemical Physics ARTICLE scitation.org/journal/jcp

# Quasielastic neutron scattering studies on couplings of protein and water dynamics in hydrated elastin

Cite as: J. Chem. Phys. 152, 245101 (2020); doi: 10.1063/5.0011107
Submitted: 17 April 2020 • Accepted: 3 June 2020 •
Published Online: 30 June 2020



Kerstin Kämpf,[1] Dominik Demuth,[1] Michaela Zamponi,[2] Joachim Wuttke,[2] and Michael Vogel[1,a)]

## AFFILIATIONS

[1] Institute of Condensed Matter Physics, Technische Universität Darmstadt, Hochschulstraße 6, 64289 Darmstadt, Germany
[2] Forschungszentrum Jülich GmbH, Jülich Centre for Neutron Science at Heinz Maier-Leibnitz Zentrum, Lichtenbergstraße 1, 85747 Garching, Germany

[a)] **Author to whom correspondence should be addressed:** michael.vogel@physik.tu-darmstadt.de

## ABSTRACT

Performing quasielastic neutron scattering measurements and analyzing both elastic and quasielasic contributions, we study protein and water dynamics of hydrated elastin. At low temperatures, hydration-independent methyl group rotation dominates the findings. It is characterized by a Gaussian distribution of activation energies centered at about $E_m$ = 0.17 eV. At ~195 K, coupled protein–water motion sets in. The hydration water shows diffusive motion, which is described by a Gaussian distribution of activation energies with $E_m$ = 0.57 eV. This Arrhenius behavior of water diffusion is consistent with previous results for water reorientation, but at variance with a fragile-to-strong crossover at ~225 K. The hydration-related elastin backbone motion is localized and can be attributed to the cage rattling motion. We speculate that its onset at ~195 K is related to a secondary glass transition, which occurs when a $\beta$ relaxation of the protein has a correlation time of $\tau_\beta \sim 100$ s. Moreover, we show that its temperature-dependent amplitude has a crossover at the regular glass transition $T_g$ = 320 K of hydrated elastin, where the $\alpha$ relaxation of the protein obeys $\tau_\alpha \sim 100$ s. By contrast, we do not observe a protein dynamical transition when water dynamics enters the experimental time window at ~240 K.



## I. INTRODUCTION

Protein functions crucially depend on manifold transitions between different molecular conformations, which, in turn, are intricately related to fluctuations of hydration water.[1–5] The microscopic mechanisms enabling protein flexibility are, however, still under vigorous debate. It was proposed that water either slaves[6] or plasticizes[7] proteins. In addition, a mutual influence of protein and water dynamics was conjectured.[8] Large parts of this controversy result from the fact that proteins exhibit various types of conformational motions on diverse time and length scales, which couple differently to water dynamics.[3,4]

Proteins show cage rattling motions inside local energy minima at short times and small lengths. Localized relaxations, e.g., side-group motions, entail somewhat larger scales, typically several picoseconds and a few angstroms at ambient temperatures. Domain motions and segmental relaxation take place at long times and involve several energy minima and, thus, large displacements. Likewise, different water species can be distinguished. Aside from free water, which resides at larger distances to protein molecules and shows bulk-like dynamics, hydration water is located at the protein surfaces and has slower dynamics. In addition, each water species exhibits several dynamical modes, in particular, structural ($\alpha$) and secondary ($\beta$) relaxations resembling those of glass-forming liquids.[9–12] Manifold relations between protein and water motions were proposed. For example, it was conjectured that local protein dynamics are slaved by fluctuations of hydration water, while large-amplitude protein dynamics are slaved by fluctuations of free water.[6]

Valuable information about couplings between relaxation processes is available when the temperature dependence of the respective relaxation times is compared. Broadband dielectric spectroscopy (BDS) and nuclear magnetic resonance (NMR) proved to be suitable methods for this purpose.[11–29] Very complex relaxation

scenarios comprising various modes of protein and water reorientations were generally observed. Although the microscopic origins of several modes remain controversial, most workers agreed that water reorientation is very similar in the hydration shells of various proteins.[9–12] Moreover, differential scanning calorimetry (DSC) studies revealed a glass transition-like phenomenon,[3,4] which was denoted as a protein glass transition. The glass transition temperatures $T_g$ strongly differ between globular and fibrous specimen, and they significantly decrease when the hydration level $h$ is increased. Here, the value of $h$ is given as the ratio of the water and protein masses (g/g).

Neutron scattering approaches utilized the H/D cross section contrast and the sensitivity to the motional mechanism to study protein and water dynamics.[30–57] A coupled protein–water relaxation was reported, which involves restricted protein dynamics inside local energy minima linked to the hydration water translation.[7,38,42,43,58] Particular interest generated the protein dynamical transition (PDT),[30] which was also observed in Mössbauer spectroscopy.[59] The PDT is identified with a crossover in temperature-dependent mean square displacements at a transition temperature $T_d$, which occurs for hydrated proteins, but not for dry ones, and is associated with an onset of protein flexibility and, mostly, function.[6,29,31,60] However, the microscopic nature of this transition and its relation to water dynamics are still controversially discussed, although an important role of water translation appears to be generally accepted.[50,61]

The significant confusion relating to the PDT is partly due to the fact that temperature-dependent atomic mean square displacements $u^2(T)$ do not show a single, but several crossovers, each marking a sudden increase in the slope. At low temperatures, $u^2(T)$ increases linearly, as expected for harmonic motion. A first crossover can occur around $T_A \sim 125$ K. It is independent of the hydration level $h$, but dependent on the time scale of the specific experiment, $\tau_{exp}$, and commonly attributed to methyl group rotation.[33,39,62] Although a further transition was also observed for dry proteins,[51,63] it is usually argued that two transitions at higher temperatures require the existence of a hydration shell. A crossover, which is weak, often masked by the methyl group contribution, and independent of the experimental time scale, often occurs at $T_B \sim 200$ K.[33,38,48,64] A more pronounced crossover, which shows a systematic $\tau_{exp}$ dependence, is often found at $T_C \sim 240$ K.[33,47,49] The temperatures of these transitions usually vary only mildly among different proteins, although there are also exceptions.[65]

Various scenarios were proposed to explain the water-related crossovers in protein mean square displacements. Doster[33] conjectured a two-step scenario in response to the slowdown of the $\alpha$ relaxation of hydration water toward a glass transition. He identified $T_B$ with the glass transition temperature of hydration water so that the amplitude of protein cage rattling motions increases when the hydration shell softens at $T_g$, resembling the situation for other glass formers.[66] Moreover, he linked $T_C$ to the PDT at $T_d$ and proposed that the crossover occurs when the $\alpha$ relaxation of hydration water enters the experimental time window, consistent with the observed $\tau_{exp}$ dependence of the phenomenon. Ngai *et al.*[11,64] related $T_B$ to the glass transition temperature $T_g$ of the respective protein–water system, where caged molecular dynamics associated with the nearly constant loss change. Moreover, they also linked $T_C$ to the PDT at $T_d$, but put forward that the Johari–Goldstein (JG) $\beta$ relaxation of hydration water[12] rather than its $\alpha$ relaxation enters the experimental time window. Hence, the observation that the crossover temperatures $T_B \sim 200$ K and $T_C \sim 240$ K differ little is traced back to the comparable $T_g$ values of the studied proteins and the similar JG $\beta$ relaxation times $\tau_\beta$ in the hydration shells of various proteins. Nevertheless, we emphasize that, irrespective of the detailed origin of both crossovers, the temperatures $T_B \sim 200$ K and $T_C \sim 240$ K should be taken as rough guides for their location rather than defining criteria, in particular, because a systematic dependence on the experimental time scale is a hallmark of the PDT, i.e., it occurs at lower temperatures for smaller $\tau_{exp}$ values. Other workers did not consider a two-step scenario and argued that the PDT occurs in response to a proposed liquid–liquid phase transition of water near 225 K.[17,45,67] In support of the slaving model, Frauenfelder *et al.*[3,6] took a somewhat different approach and showed that the decrease in protein elastic scattering intensities with increasing temperature can be rationalized based on the speedup of water dynamics in the hydration shell, which they denoted as $\beta_h$ fluctuations. Interestingly, a PDT was also observed for hydrated amino acids, which was taken as evidence that the phenomenon is water driven.[52]

Here, we exploit that small globular proteins and large fibrous proteins have different glass transition temperatures $T_g$. While neutron scattering works increasingly focused on complex proteins or even living cells in the last decade,[53–57] many basic approaches employed small model proteins, which show $T_g \sim 200$ K in their hydrated states. Examples are myoglobin,[13,17] lysozyme,[16,68] and bovine serum albumin.[15] By contrast, we investigate the fibrous protein elastin, which has a glass transition temperature of $T_g \sim 320$ K at $h \geq 0.2$ g/g.[20,24] While $T_g$ is much higher for elastin than for the above globular proteins, the correlation times of water dynamics are very similar in the hydration shells of all these proteins,[26] allowing us to test the above discussed models of protein–water couplings.

Elastin is a main component of connective tissue, which is formed out of tropoelastin by post-translational modification. It features hydrophobic domains between hydrophilic crosslinks and differs from common model proteins due to its higher molecular weight, its higher fraction of hydrophobic amino acids, and the fact that large parts of elastin lack defined secondary structure motifs and have random-coil conformation.[21] Several studies showed that elastin and water dynamics are enhanced upon hydration.[19–27] In particular, glass transition temperatures and rotational correlation times decrease up to $h \approx 0.2$ g/g, while they are unchanged at higher hydration levels, where unfrozen hydration water coexists with frozen free water at cryogenic temperatures.[20,24] Thus, a hydration level of $h = 0.2$ g/g is particularly suited for studies on couplings of elastin and water dynamics. Up to three BDS relaxation processes of hydrated elastin were reported. The fastest one can be attributed to hydration water[19–27] and described by a Gaussian distribution of activation energies.[23] The intermediate and slow processes were assigned to noncooperative and cooperative dynamics of the elastin–water system, respectively.[21,24] Molecular dynamics simulations of hydrated elastin-like polypeptides revealed power-law-like decays of correlation functions associated with hydration-dependent backbone motions on pico-to nanosecond scales.[28,69,70]

We perform neutron scattering studies on protein and water dynamics in dry and hydrated ($h = 0.2$ g/g) elastin to shed new light

on coupled protein–water motions. To discriminate between protein and water contributions, we exploit the H/D incoherent scattering contrast and compare results for samples hydrated by either $H_2O$ or $D_2O$. Over broad temperature ranges, we analyze the elastic intensities to obtain mean square displacements, and we determine the quasielastic intensity at a fixed frequency,[71,72] providing access to mobility distributions.[40,73,74]

## II. MATERIALS AND METHODS

### A. Sample preparation

We investigate elastin in the dry state, elastin hydrated by $H_2O$ (ELA-$H_2O$), and elastin hydrated by $D_2O$ (ELA-$D_2O$). The hydration level of the latter two samples was set to $h$ = 0.2 g/g, ensuring that there is a complete hydration shell, while freezable free water is still absent. In the supplementary material, we show additional experimental results for a hydration level of $h$ = 0.4 g/g, where a fraction of water crystallizes. Elastin from the bovine neck ligament was purchased from Sigma-Aldrich and used without further purification. It has a molecular weight of ~64 kDa. For sample preparation, elastin was first dried under weak vacuum at ambient temperature for more than 12 h. The, thus, obtained dry protein was then hydrated in a controlled manner by exposure to saturated KCl–$H_2O$ atmosphere (ELA-$H_2O$) or pure $D_2O$ atmosphere (ELA-$D_2O$). The hydration level was determined by measuring the mass change upon water uptake. For neutron scattering measurements, the dry and hydrated elastin samples were placed in flat aluminum sample holders. The sample thickness amounted to only 0.2 mm to minimize effects of multiple scattering.

The present experimental results are dominated by the incoherent scattering of protons in the studied samples. Therefore, Table I specifies the fractions of various proton species, as estimated based on results for the amino acid sequence of elastin.[75] 31% and 69% of elastin protons do and do not belong to methyl groups, respectively. The latter can be further divided into exchangeable and nonexchangeable protons. Assuming that each amino acid, except proline, has one exchangeable proton, ELA-$H_2O$ ($h$ = 0.2 g/g) features 10% exchangeable non-methyl protein protons. Supposing that the latter fraction is statistically distributed between water and elastin by H/D exchange in ELA-$D_2O$, we expect that there are ~9% water protons in this sample.

**TABLE I**. Proton fractions in the studied samples. We distinguish between water protons, methyl protons, and non-methyl protein protons. The latter fraction contains ~10% exchangeable protons, which are distributed between protein and water by H/D exchange in ELA-$D_2O$.

| | | Protein protons | |
|---|---|---|---|
| | Water protons | Methyl | Non-methyl |
| dry elastin | ... | 0.31 | 0.69 |
| ELA-$H_2O$ | 0.23 | 0.24 | 0.53 |
| ELA-$D_2O$ | ~0.09 | 0.31 | ~0.60 |

### B. Neutron scattering

Incoherent neutron scattering measurements were performed on the backscattering spectrometer SPHERES operated by the Jülich Centre for Neutron Science at the Heinz Maier-Leibnitz Zentrum (MLZ, Garching, Germany).[76,77] It has an energy resolution of $\Delta E$ = 0.65 $\mu$eV (full width at half maximum) and provides access to scattering vectors $q$ between 0.2 Å$^{-1}$ and 1.8 Å$^{-1}$. Due to a low signal-to-noise ratio of the small-angle detectors, the present analysis was, however, restricted to the range $q$ = 0.6–1.8 Å$^{-1}$. Measurements in the energy range of $-4.68\ \mu\text{eV} < \hbar\omega < 4.68\ \mu\text{eV}$ were performed between 4 K and 360 K. More precisely, we used temperature ramps of 22 K/h for dry elastin and of 15 K/h below 100 K and 7.5 K/h above 100 K for hydrated elastin and binned data at time intervals of 20 min.

Figure 1 shows exemplary data of the measured dynamic structure factors $S(q, \omega, T)$. Results of ELA-$H_2O$ for the scattering vector $q$ = 0.6 Å$^{-1}$ at three characteristic temperatures are compared. In the following analyses, we utilize the experimental results to determine both the elastic intensity $S(q, \omega = 0, T)$ and the quasielastic energy at a fixed frequency $\omega_f$, $S(q, \omega = \omega_f, T)$, where $\hbar\omega_f$ = 2.25 $\mu$eV. More precisely, to improve the signal-to-noise ratio, we approximate $S(q, \omega = \omega_f, T)$ by the average intensity $I(q, \omega \approx \omega_f, T)$ of the dynamic structure factor in the ranges $1.5\ \mu\text{eV} < |\hbar\omega| < 3\ \mu\text{eV}$; see Fig. 1. To refer to contributions $S(q, \omega = \omega_f, T)$ in a predefined frequency/energy window, the term inelastic fixed window (IFW) intensity was coined.[71]

Neglecting contributions from finite experimental resolution and vibrational atomic motion, the dynamic structure factor can be written as[78]

$$S(q, \omega, T) = A_0(q)\delta(\omega) + [1 - A_0(q)]L(q, \omega, T). \quad (1)$$

Here, $A_0(q)$ denotes the elastic incoherent structure factor and $L(q, \omega, T)$ describes the quasielastic components. Moreover, assuming simple molecular dynamics described by exponential correlation functions, the IFW intensity is given by

$$S(q, \omega_f, T) \propto [1 - A_0(q)]\,\frac{\tau(q, T)}{1 + [\omega_f \tau(q, T)]^2}. \quad (2)$$

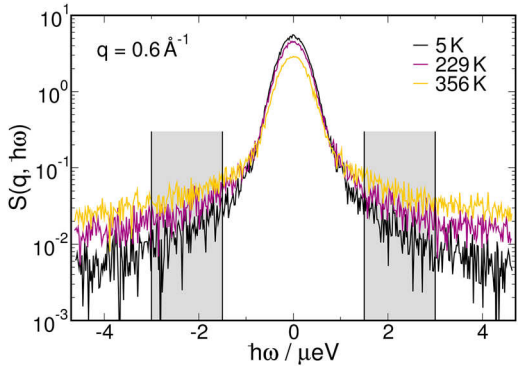


**FIG. 1**. $S(q, \hbar\omega)$ of ELA-$H_2O$ for $q$ = 0.6 Å$^{-1}$ at characteristic temperatures. The energy ranges $1.5\ \mu\text{eV} < |\hbar\omega| < 3\ \mu\text{eV}$ used to determine the IFW intensity are indicated as gray shaded areas.

In temperature-dependent analyses, the IFW intensity shows a maximum when the correlation time $\tau$ of the motion obeys $\omega_f \tau = 1$. This maximum occurs because the Lorentzian function $L(q, \omega, T)$ associated with such molecular dynamics is too broad at high temperatures, where $\tau$ is short, and too narrow at low temperatures, where $\tau$ is long, to produce high intensity at $\omega_f$. Using $\hbar\omega_f \cong 2.25\ \mu$eV, the present IFW studies probe molecular dynamics at a time scale of ~0.3 ns. Different types of motions can be discriminated when the IFW intensity is analyzed for various scattering vectors $q$. While the position of the maximum is independent of the scattering vector for localized dynamics, a $q$ dependence results from diffusive motions.[78]

For hydrated elastin, we expect that the prominent disorder in the structure results in a strong heterogeneity of the dynamics. To consider such dynamical heterogeneity in disordered materials, it is useful to assume a temperature-independent Gaussian distribution of activation energies,[23,79–81]

$$G(E) = \frac{1}{\sqrt{2\pi}\sigma} \exp\left[-\frac{(E - E_m)^2}{2\sigma^2}\right], \tag{3}$$

which is characterized by a mean value $E_m$ and a standard deviation $\sigma$. For $q$-independent thermally activated motions, the corresponding temperature-dependent distributions of correlation times can be calculated using the Arrhenius law,

$$\tau(E, T) = \tau_0 \exp\left(\frac{E}{k_B T}\right). \tag{4}$$

Under such circumstances, the IFW intensity is given by

$$S(\omega_f, T) \propto \int_0^\infty G(E) \frac{\tau(E, T)}{1 + [\omega_f \tau(E, T)]^2}\, dE. \tag{5}$$

We will use this model to account for methyl group reorientation.

To describe IFW contributions from diffusive motion governed by a Gaussian distribution of activation energies $G(E)$, we apply the Arrhenius law to obtain distributed diffusion coefficients,

$$D(E, T) = D_0 \exp\left(-\frac{E}{k_B T}\right). \tag{6}$$

Then, the IFW intensity can be written as

$$S(q, \omega_f, T) \propto \int_0^\infty G(E) \frac{D(E, T) q^2}{[D(E, T) q^2]^2 + \omega_f^2}\, dE, \tag{7}$$

where it is exploited that correlation times and diffusion coefficients are related by $\tau^{-1}(q) = Dq^2$.

The elastic intensity $S(q, \omega = 0, T)$ is employed to determine mean square displacements $u^2(T)$. Specifically, elastic energy and atomic displacements are related by[82]

$$u^2(T) = \lim_{q^2 \to 0}\left[-\frac{3}{q^2} \ln \frac{S(q, \omega = 0, T)}{S(q, \omega = 0, T = 4\,\mathrm{K})}\right], \tag{8}$$

where the low-temperature result $S(q, \omega = 0, T = 4\ \mathrm{K})$ in the denominator ensures appropriate normalization. At SPHERES, this analysis probes molecular displacements at a fixed time scale of $\tau_{exp} = 2$ ns, as determined by the energy resolution of this setup. More detailed information about the evaluation of the elastic intensity and the determination of the mean square displacement can be found in the supplementary material.

## III. RESULTS

### A. IFW intensity of dry elastin

First, we study the temperature-dependent IFW intensity of dry elastin. Figure 2 presents results for scattering vectors $q$ in the range 0.6 Å$^{-1}$–1.8 Å$^{-1}$. Independent of the value of $q$, the IFW intensity starts to increase at $T \sim 125$ K and passes a maximum at $T \sim 220$ K. As aforementioned, an IFW intensity maximum results because $S(q, \omega, T)$ is too narrow to produce high intensity at $\omega = \omega_f$ when dynamics is slow at low temperatures, while it is too broad when dynamics is fast at high temperatures. A lack of $q$ dependence shows that the underlying dynamics is localized rather than diffusive. Previous neutron scattering approaches to proteins reported that methyl group rotation results in IFW intensity maxima, which do not depend on the value of $q$ and occur at similar temperatures.[40,73] Following these studies, we assign the observed IFW intensity to methyl group reorientation. For a quantitative analysis, we assume that the disorder in the local environments causes distributions of activation energies and, thus, of correlation times for this motion. We find that a temperature-independent Gaussian distribution of activation energies $G(E)$ in combination with an Arrhenius law, see Eq. (5), enables a successful interpolation of the data. When we exploit knowledge from previous works[40,73,83] and fix $\tau_0$ at $10^{-13}$ s, this fit approach yields a mean activation energy of $E_m = 0.17$ eV and a standard deviation of $\sigma = 0.04$ eV. These results are in excellent agreement with previous findings for methyl group rotation of other proteins and polypeptides.[40,58,72,73]

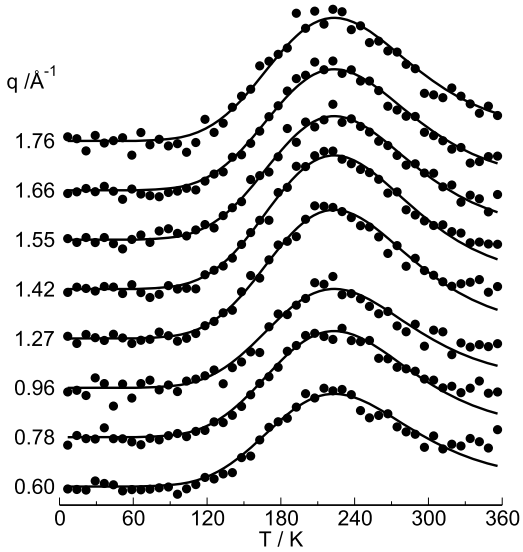


**FIG. 2.** Temperature-dependent IFW intensity $I(q, \omega_f, T)$ of dry elastin for the indicated scattering vectors $q$ between 0.60 Å$^{-1}$ and 1.76 Å$^{-1}$. As explained in Sec. II B, these and the following $I(q, \omega_f, T)$ data are obtained from averaging the dynamic structure factor in energy ranges around $\hbar\omega_f = 2.25\ \mu$eV; see Fig. 1. For clarity, $I(q, \omega_f, T)$ data for various scattering vectors are shifted along the vertical axis. The lines indicate a global fit of the results for all studied $q$ values, which is based on a Gaussian distribution of activation energies $G(E)$, see Eq. (5), yielding a mean value of $E_m = 0.17$ eV and a standard deviation of $\sigma = 0.04$ eV.

### B. IFW intensity of hydrated elastin

Next, we study the influence of hydration on the IFW intensity. In Fig. 3, we compare data of elastin in the dry state with those of elastin hydrated by $H_2O$ or $D_2O$ for three exemplary scattering vectors. Below about ~195 K, the IFW intensity is independent of hydration. As the experimental findings at low temperatures are dominated by methyl group rotation, the independence reveals that this motion is not affected by hydration, consistent with previous results.[28,44,58,72] Above ~195 K, hydration leads to enhanced IFW intensity, whereby the effect is stronger for ELA-$H_2O$ than for ELA-$D_2O$. The latter finding indicates that dynamics of hydration water contributes to the experimental results in this temperature range. This argument can be deduced when we consider the facts that the incoherent scattering cross section is much higher for protons than deuterons and that the H/D ratio is larger in the hydration water of ELA-$H_2O$ than in that of ELA-$D_2O$; see Table I. Consequently, the IFW intensity receives higher contributions from water dynamics for ELA-$H_2O$ than for ELA-$D_2O$, explaining the observed discrepancies. However, this does not mean that the differences between the dry and hydrated samples are exclusively due to water dynamics, as will be explored below.

#### 1. Water dynamics

Before turning to that topic, we investigated water dynamics in more detail by subtracting the IFW intensity of ELA-$D_2O$ from that of ELA-$H_2O$. This analysis assumes that observable protein dynamics are the same in both samples, and it neglects minor effects arising from a weak mismatch of $H_2O$ and $D_2O$ dynamics. The temperature-dependent difference curves resulting from such a subtraction are shown for various scattering vectors $q$ in Fig. 4. We observe no difference below ~195 K, where ELA-$D_2O$ and ELA-$H_2O$ have similar IFW intensities, see Fig. 3, whereas the difference curves show maxima near 300 K, indicating that water dynamics crosses the time scale (~0.3 ns) of our IFW analysis.

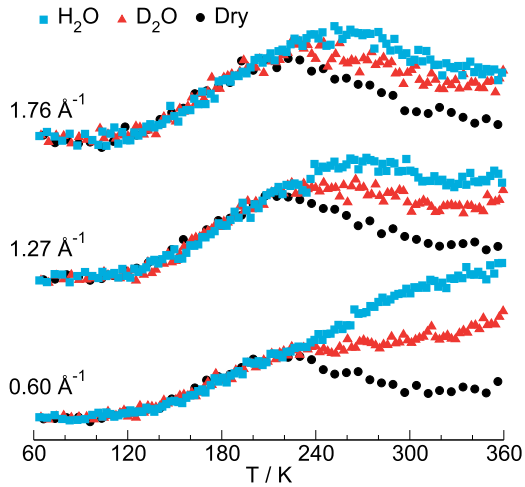


**FIG. 3**. Comparison of the temperature-dependent IFW intensities $I(q, \omega_f, T)$ of dry elastin, ELA-$H_2O$, and ELA-$D_2O$. Results for the indicated exemplary scattering vectors $q$ and $\hbar\omega_f \cong 2.25$ $\mu$eV are shown.

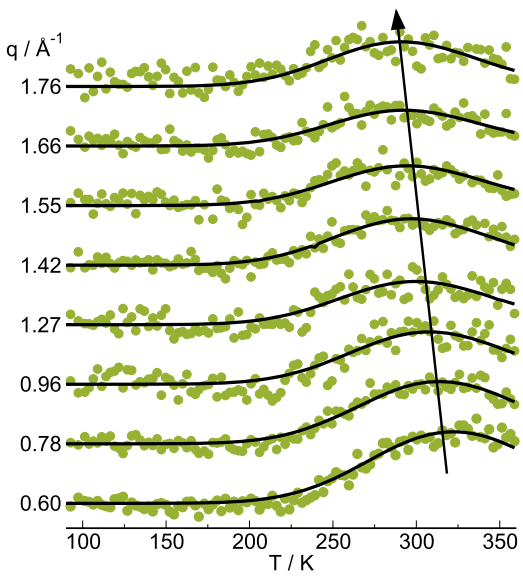


**FIG. 4**. Temperature-dependent IFW intensity of the hydration water of elastin for the indicated scattering vectors $q$ between 0.60 Å$^{-1}$ and 1.76 Å$^{-1}$. The data were obtained by subtracting $I(q, \omega_f, T)$ of ELA-$D_2O$ from that of ELA-$H_2O$; see Fig. 3. The arrow indicates that the intensity maximum shifts to lower temperatures when the scattering vector is increased. The lines indicate a global fit of the results for all studied $q$ values to the model of diffusive motion governed by a Gaussian distribution of activation energies $G(E)$, see Eq. (7), yielding a mean value of $E_m = 0.57$ eV and a standard deviation of $\sigma = 0.08$ eV.

Unlike the peaks of the methyl group contribution, the maxima due to hydration water dynamics shift to lower temperatures when the value of $q$ is increased. The observed $q$ dependence is indicative of diffusive motion.[71,78] Therefore, we analyze these data based on Eq. (7), which assumes diffusion governed by a Gaussian distribution of activation energies $G(E)$. In Fig. 4, we see that this model allows successful global interpolations of the data for all studied scattering vectors $q$, confirming the diffusive nature of the observed water motion. We note that, unlike in the above evaluation of methyl group dynamics, stable fits are obtained when the pre-exponential factor is treated as a free parameter rather than a fixed parameter, yielding $D_0 = 0.06$ m$^2$/s.

The Gaussian distribution of activation energies $G(E)$ resulting from this analysis of hydration water diffusion is described by a mean value of $E_m = 0.57$ eV and a standard deviation of $\sigma = 0.08$ eV. In Fig. 5, we observe that this result for translational dynamics agrees with previous findings for rotational dynamics of elastin hydration water.[21–26] Explicitly, combined BDS and NMR studies yielded a Gaussian distribution $G(E)$ with similar parameters, $E_m = 0.55$ eV and $\sigma = 0.04$ eV.[23] Thus, translational and rotational dynamics of elastin hydration water are described by consistent Arrhenius behaviors. In particular, we see in Fig. 5 that the inverse of the peak diffusion coefficient $D_m$ calculated from the mean activation energy $E_m$ according to Eq. (6) has a very similar temperature dependence to peak rotational correlation times $\tau$ found in previous BDS and NMR studies.[21,24,26] All these results are at variance with a fragile-to-strong crossover in response to a

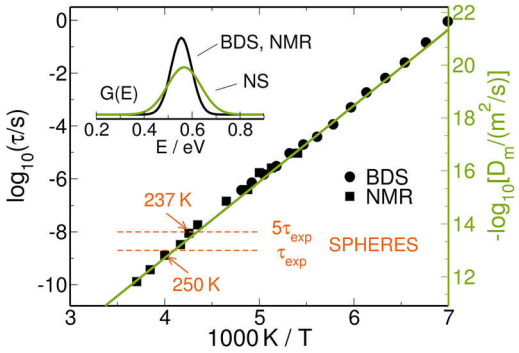


**FIG. 5**. Comparison of present and previous findings for the dynamics of elastin hydration water. The main panel shows temperature-dependent diffusion coefficients and correlation times, and the inserted panel compares distributions of activation energies. Specifically, the inverse diffusion coefficients $D_m$ (line) obtained in the present approach from the mean activation energy $E_m$ according to Eq. (6) are displayed together with rotational correlation times $\tau$ (symbols) reported in BDS and NMR works.[21,24–26] Furthermore, the Gaussian distribution $G(E)$ of our study ($E_m$ = 0.57 eV, $\sigma$ = 0.08 eV) is presented together with that of combined BDS and NMR analyses on the dynamics of elastin hydration water ($E_m$ = 0.55 eV, $\sigma$ = 0.04 eV).[23] The arrows indicate the temperatures 237 K and 250 K, where the rotational correlation times of elastin hydration water enter the experimental time window of the SPHERES setup, explicitly, where $\tau = \tau_{exp}$ and $\tau = 5\tau_{exp}$, respectively.

liquid–liquid phase transition, which was reported in a previous neutron scattering work on protein hydration waters and related to the PDT.[45,47]

### 2. Elastin dynamics

Next, we use the IFW intensity to gain insights into elastin motions other than methyl group rotation. For this purpose, we determine intensity beyond that contributed by methyl and water protons, which are known from the above analyses. In Fig. 6, the

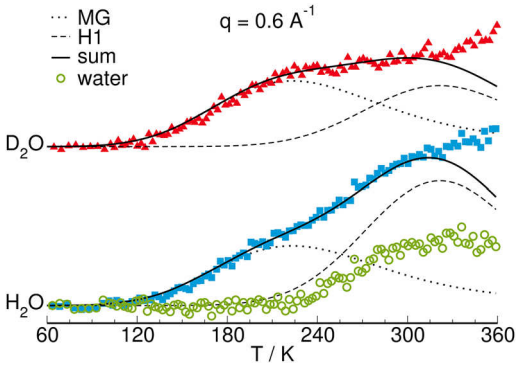


**FIG. 6**. Temperature-dependent IFW intensity $I(q, \omega_f, T)$ of (bottom) ELA-$H_2O$ and (top) ELA-$D_2O$ for $q$ = 0.60 Å$^{-1}$ and $\hbar\omega_f \cong 2.25$ $\mu$eV. The solid line is the sum of the contribution of methyl group reorientation (MG, dotted lines) and an upscaled contribution from hydration water dynamics (H1, dashed lines), which were calculated from the fits in Figs. 2 and 4, respectively. The actual, i.e., the unscaled water contribution, as obtained by subtracting the IFW intensity of ELA-$D_2O$ from that of ELA-$H_2O$, is shown for comparison (open circles).

situation is illustrated for both hydrated samples and an exemplary scattering vector $q$. For ELA-$H_2O$, we find that the total IFW intensity differs from the sum of the methyl and water contributions above ~195 K, indicating that elastin motions other than methyl dynamics cause additional intensity. Notwithstanding, the total intensity is well described up to ~320 K by a superposition of the methyl group contribution and an *upscaled*, i.e., *weighted* water contribution, which we denote as H1 contribution. In this analysis, the superposition is based on the model functions calculated from the above determined $G(E)$ distributions of methyl group and hydration water motions. Likewise, for ELA-$D_2O$, a superposition of the methyl group and H1 contributions well interpolates the total IFW intensity below ~320 K. However, the H1 contribution is again much higher than expected based on the small fraction of water protons in this sample; see Table I. These findings imply that elastin shows dynamics, which occurs on the same time scale as water motion and adds to the H1 contribution. Hence, our results are consistent with coupled protein–water dynamics reported in the literature.[7,38,42,43,58] Above 320 K, the superpositions of the methyl group and H1 contributions, however, do no longer describe the total IFW intensities of ELA-$H_2O$ and ELA-$D_2O$. Specifically, another IFW contribution, to which we refer to as H2 contribution, grows when heating in this temperature range. This observation indicates that either the properties of the coupled elastin–water dynamics, e.g., its amplitude, change at ~320 K or another type of elastin dynamics sets in; see below.

For a more detailed study of the latter elastin motion, we subtract the above determined superpositions of methyl and H1 contributions from the total IFW intensities. The resulting temperature-dependent H2 contribution is displayed in Fig. 7. We observe that the H2 contributions of ELA-$H_2O$ and ELA-$D_2O$ agree for all $q$, confirming successful removal of water contributions, which, otherwise, would cause deviations due to their very different magnitudes in these samples. Hence, the results reflect elastin dynamics other than methyl group rotation. The H2 contribution is negligible below ~320 K, whereas it increases continuously when heating above this temperature. The onset of this increase hardly depends on the value of $q$. This may suggest that the probed elastin motion is of local nature, but, unfortunately, detailed analysis of this protein dynamics is not possible, because it does not produce an IFW intensity maximum in the studied temperature range up to 360 K. Nevertheless, it is remarkable that the H2 contribution starts to grow near the glass transition temperature $T_g \sim 320$ K.[20,24]

## C. Mean square displacement of dry and hydrated elastin

We turn our attention to the mean square displacements $u^2(T)$ determined from the elastic intensities using Eq. (8); see the supplementary material. In Fig. 8, we observe that hydration does not affect $u^2(T)$ below ~195 K. In particular, for both dry and hydrated elastin, $u^2(T)$ shows a crossover at $T_1 \sim 125$ K, which can be attributed to the onset of the methyl group rotation on the experimental time scale.[7,44,48,62] By contrast, hydration results in enhanced mean square displacements above $T_2 \sim 195$ K. More precisely, the slope of $u^2(T)$ remains essentially unchanged up to 360 K for dry elastin, whereas it is larger at $T > T_2$ and further increases at $T_3 \sim 320$ K for the hydrated samples. In passing, we note that these results for a

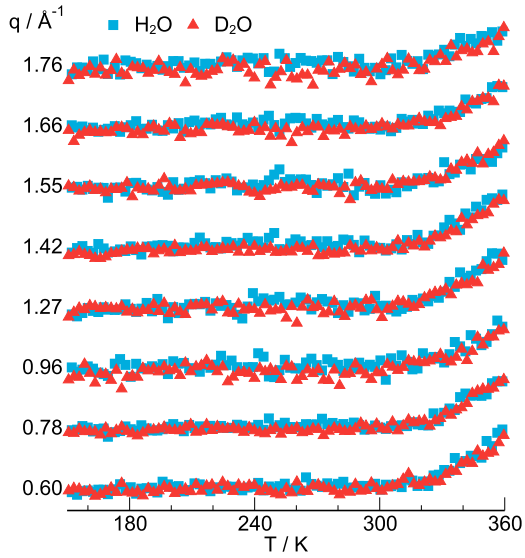


**FIG. 7**. Temperature-dependent IFW intensity resulting from elastin dynamics other than methyl group reorientation for the indicated scattering vectors $q$ between 0.60 Å$^{-1}$ and 1.76 Å$^{-1}$. Results for ELA-$H_2O$ and ELA-$D_2O$ are compared. The data were obtained by subtracting weighted superpositions of contributions from methyl group reorientation, see Fig. 2, and hydration water dynamics (H1), see Fig. 4, from the measured total IFW intensity $I(q, \omega_f, T)$ for $\hbar\omega_f \cong 2.25$ $\mu$eV. The weighting factors were determined as illustrated in Fig. 6.

hydration level of $h = 0.2$ g/g, which allows us to avoid crystallization of water, agree with findings for $h = 0.4$ g/g up to 273 K, where $u^2(T)$ of the latter sample shows a discontinuity owing to melting of ice; see the supplementary material.

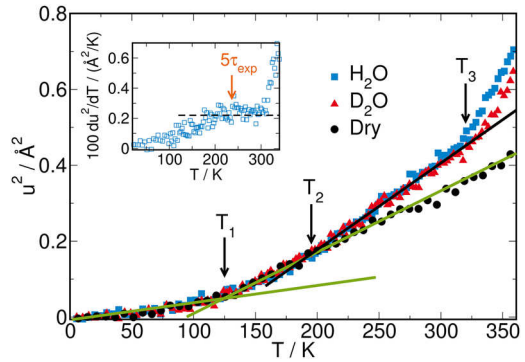


**FIG. 8**. Temperature-dependent mean square displacement $u^2(T)$ of dry elastin, ELA-$H_2O$, and ELA-$D_2O$, as obtained from fits of the elastic intensities to Eq. (8); see the supplementary material. The lines indicate approximately linear behaviors in various temperature ranges. The arrows mark crossover temperatures $T_1 \sim 125$ K, $T_2 \sim 195$ K, and $T_3 \sim 320$ K. The inset shows the numerically calculated derivative $\frac{du^2}{dT}(T)$ for ELA-$H_2O$. The horizontal dashed line indicates nearly linear behavior of $u^2(T)$ in the temperature range 195 K–320 K. The arrow marks the temperature 237 K where water rotational motion enters the experimental time window, explicitly, $\tau = 5\tau_{exp}$; see Fig. 5.

Comparing the findings for ELA-$H_2O$ and ELA-$D_2O$ in more detail, we observe similar behaviors in the range 195 K–320 K, implying that elastin dynamics decisively contributes to the enhanced mean square displacements of the hydrated samples. This is because if water dynamics were the main origin of the effect, we would observe significant differences between both hydrated samples as a consequence of their diverse fractions of water protons; see Table I. Considering the results of our IFW analyses, we propose that the enhanced displacements of the hydrated samples at $T_2 < T < T_3$ are caused by the above discussed coupled elastin–water dynamics. Moreover, we see in Fig. 8 that the $T_3$ values of ELA-$H_2O$ and ELA-$D_2O$ differ by about 5 K due to isotope effects. Yet, $u^2(T)$ increases in a similar manner for both samples above the respective crossover temperature, again suggesting major contributions from elastin dynamics. Specifically, comparison with Figs. 6 and 7 implies that the onset of the H2 contribution to the IFW intensity is related to the $T_3$ crossover.

Interestingly, the mean square displacements of hydrated elastin do not yield evidence for the much-noticed PDT occurring for many other proteins at $T_d \approx 240$ K. In particular, inspecting the inset of Fig. 8, we find that the numerically calculated derivative $\frac{du^2}{dT}(T)$ is basically constant for ELA-$H_2O$ in the range 195 K–320 K. Commonly, it is regarded as a defining criterion of the PDT that the associated $u^2(T)$ break occurs when water dynamics, be it related to $\alpha$, JG $\beta$, or $\beta_h$ fluctuations,[6,11,33] enters the time window of the experiment, e.g., when $\tau = 5\tau_{exp}$. For elastin hydration water, the latter relation is obeyed at 237 K; see Fig. 5. Therefore, we marked this temperature in the inset of Fig. 8. Evidently, when hydration water reorientation crosses the experimental time scale, there are no major changes in $u^2(T)$, which would indicate a PDT of hydrated elastin.

## IV. DISCUSSION

Analyzing elastic and quasielastic contributions to the dynamic structure factor $S(q, \omega, T)$, we ascertained several relaxation processes of dry and hydrated elastin. The fastest one could be assigned to methyl group rotation. It causes a decrease in the elastic intensity and a corresponding increase in the quasielastic intensity, which set in at $T_1 \sim 125$ K for both dry and hydrated elastin. Focusing on the temperature-dependent intensity at a fixed frequency offset, i.e., performing an IFW analysis,[71] we found that the methyl group reorientation is described by a Gaussian distribution of activation energies $G(E)$ with a mean energy of $E_m = 0.17$ eV and a standard deviation of $\sigma = 0.04$ eV, independent of the value of the scattering vector $q$. These results are in very good agreement with those for other proteins and also polypeptides,[40,58,72,73] e.g., a Gaussian distribution characterized by $E_m = 0.17$ eV and $\sigma = 0.06$ eV was found for lysozyme.

The observation that methyl group rotation is independent of the water content allowed us to eliminate this contribution from $S(q, \omega, T)$ data for hydrated elastin. In this way, we identified two hydration-dependent contributions to the IFW intensity, which we denoted as H1 and H2 contributions. The H1 contribution is dominated by water dynamics, but also receives contributions from elastin dynamics other than methyl rotation, as determined by analyzing the magnitude of this intensity. To single out effects from

water dynamics, we subtracted the IFW intensity of ELA-$D_2O$ from that of ELA-$H_2O$. The, thus, obtained difference curves start growing at ~195 K and pass a maximum near 300 K, dependent on the value of $q$, indicating diffusive water motion. The H2 contribution stems from elastin dynamics other than methyl rotation and sets in at ~320 K. Its onset appears to be independent of the scattering vector $q$, which may suggest localized motion, but its maximum is not reached in the studied temperature range up to 360 K, preventing definite conclusions about the very nature of elastin dynamics related to H2.

The IFW contribution from hydration water could be consistently described for all studied scattering vectors $q$ by assuming diffusive motion governed by a Gaussian distribution of activation energies $G(E)$ with a mean value of $E_m = 0.57$ eV and a standard deviation of $\sigma = 0.08$ eV. Consistent with the supposed diffusive nature, displacements of protein hydration waters on micrometer scales were observed in the literature.[84] Moreover, in harmony with the assumed thermally activated motion, Arrhenius laws with similar activation energies of ~0.5 eV were found for reorientation dynamics of hydration water of various proteins.[11–26] In particular, Gaussian distributions with $E_m \approx 0.54$ eV and $\sigma \approx 0.04$ eV were obtained for the fibrous proteins elastin and collagen.[23] These results indicate that translational and rotational dynamics of elastin hydration water are governed by a common $G(E)$ distribution; see Fig. 5. Moreover, they show that water dynamics are similar in the hydration shells of both globular and fibrous proteins. The similar behavior, which involves, if any, only weak deviations from Arrhenius behavior, is evident when we compare the rotational correlation times of elastin hydration water with those of other protein hydration waters in Fig. 9. It should, however, be noted that, at variance with these findings, other neutron scattering works reported a fragile-to-strong crossover for protein hydration waters at ~225 K.[45,47]

To obtain further information about hydration-related elastin dynamics, we compared elastic incoherent neutron scattering data of dry and hydrated samples. This analysis was done based on the related mean square displacements $u^2(T)$ at the fixed experimental time scale of $\tau_{exp} = 2$ ns; see Eq. (8). All studied samples share a common $u^2(T)$ behavior associated with hydration-independent methyl group reorientation up to $T_2 \sim 195$ K, whereas hydrated elastin shows increasingly larger mean square displacements than dry elastin when heated above this temperature. In particular, ELA-$H_2O$ and ELA-$D_2O$ exhibit a $u^2(T)$ crossover at $T_3 \sim 320$ K, mildly dependent on the isotope, which does not occur in the dry state.

Thus, several phenomena concur for hydrated elastin at $T_3 \sim 320$ K. While we revealed a crossover in $u^2(T)$ and an onset of the H2 contribution at this temperature, other workers reported that the glass transition temperature of hydrated elastin amounts to $T_g \sim 320$ K.[20,24] In view of this coincidence, we follow previous works on hydrated proteins[11,49] and attribute the observed changes of elastin dynamics at $T_3 \approx T_g \sim 320$ K to a higher temperature dependence of the amplitude of caged dynamics above the glass transition temperature, resembling the situation for various types of glass formers and reflecting a change in the temperature evolution of the density owing to vitrification.[66] Such localized dynamics is also consistent with the observation that the H2 contribution shows no clear $q$ dependence. Under such circumstances, the absence of an analogous crossover for dry elastin in the studied temperature range can be rationalized based on its higher glass transition temperature of $T_g = 470$ K.[20] In other words, we propose that the main cause for the different dynamical behaviors observed for the dry and hydrated samples in the range 320 K–360 K is the fact that the dry protein is in the glassy state ($T < T_g$) in this temperature range, while the hydrated one is in the viscous state ($T > T_g$) because water acts as a plasticizer and reduces the glass transition temperature of elastin. At this stage, it should, however, be mentioned that hydrated elastin shows a much debated inverse temperature transition at ~310 K.[85,86] Despite occurring also near 320 K, we do not regard the latter phenomenon as important in the present context, because it marks a transition to a more folded state upon heating and, hence, should result in lower rather than higher atomic displacements.

Several neutron scattering studies on protein dynamics observed a crossover in temperature-dependent mean square displacements at $T_B \sim 190$ K–210 K, which does not depend on the

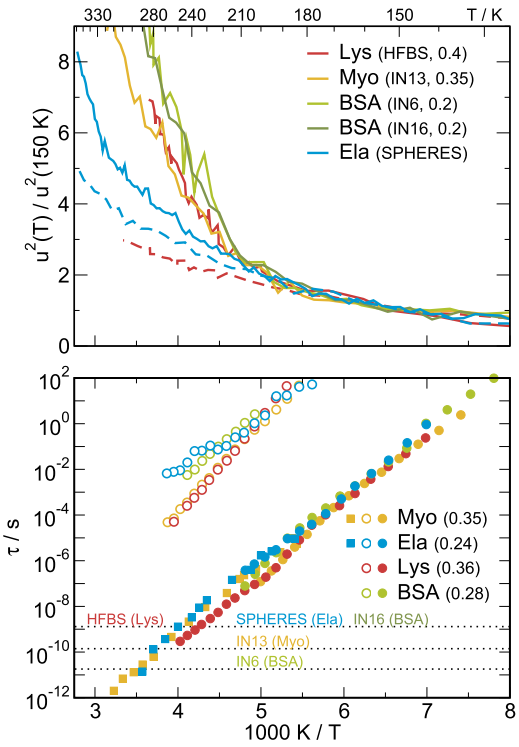


**FIG. 9.** Temperature dependence of (top) mean square displacements $u^2$ and (bottom) rotational correlation times $\tau$ of protein–water systems. To eliminate discrepancies due to differing analysis procedures, the mean square displacements are scaled, $u^2(T)/u^2(T = 150\ K)$, such that they agree at the temperature of 150 K, where the findings are dominated by methyl group reorientation. Literature results for lysozyme,[41] myoglobin,[34] and bovine serum albumin[48] are included. Dashed curves are mean square displacements of dry elastin and lysozyme. The rotational correlation times are from BDS (circles) and NMR (squares) studies. Fast and slow BDS relaxation processes are distinguished using solid and open symbols, respectively. Results for elastin,[24,25] lysozyme,[16] myoglobin,[16,26] and bovine serum albumin[15] are compared. In brackets, the used neutron scattering spectrometers and hydration levels are specified. The horizontal dotted lines indicate the respective experimental time scales $\tau_{exp}$.

experimental time window.[17,33,34,40,48,49] This effect may not be mistaken with a further crossover, which, systematically depending on the spectrometer resolution, occurs at $T_C \sim 230$ K–250 K and is usually attributed to the PDT at $T_d$. For hydrated proteins, the crossover at ~200 K was assigned to an increasing amplitude of cage rattling motions when the material softens during a glass transition of water[33] or protein.[49] This assignment was motivated by analogies with other glass formers[66] and based on the observation of DSC and BDS signatures of the studied globular proteins in this temperature range. However, a combination of neutron scattering with DSC and BDS studies revealed for myoglobin that the $u^2(T)$ crossover temperature remains unchanged when the glass transition temperatures $T_g$ and rotational correlation times $\tau$ vary upon increasing the hydration level,[17] indicating that there is no stringent relation between $T_B$ and $T_g$. Likewise, the crossover temperature $T_B$ does not depend on the value of $h$ for lysozyme,[40] while the $T_g$ value does.[16] This change in $u^2(T)$ at $T_B$ is usually weaker for lower hydration levels $h$. For dry proteins, the effect is, consistently, very weak but still discernible and was attributed to thermal activation of collective anharmonic motions, which enhance protein flexibility,[51] or, alternatively, to a change in cage rattling dynamics when crossing a secondary glass transition temperature $T_{g,\beta}$, where the JG $\beta$ relaxation has a correlation time of ~100 s.[63] For a simple glass former, the results of a detailed neutron scattering study implied that the amplitude of overdamped vibrational motion changes as a result of thermally activated transitions between metabasins in the energy landscape, which are associated with the JG $\beta$ relaxation.[87]

To further discuss previous and present findings associated with the onset of hydration-related protein dynamics at ~200 K, we compare not only rotational correlation times but also mean square displacements in Fig. 9. In detail, the comparison includes data for the globular proteins myoglobin, lysozyme, and bovine serum albumin in addition to our results for fibrous elastin. The hydration levels of all samples are in the range $h = 0.2$–$0.4$ g/g, where the hydration shells are already filled, while freezable water is still absent. We see that all hydrated proteins show similar rotational and translational dynamics. Specifically, they share faster and slower relaxation processes in BDS studies, and they exhibit a common onset of hydration-enhanced displacements at $T_B \sim T_2 \sim 190$ K–210 K in neutron scattering approaches.

The faster BDS process, as discussed above, results from similar water reorientation in the hydration shells of various proteins. The slower BDS process was attributed to the $\alpha$ relaxation of proteins,[4,11,16] because it has correlation times of $\tau \sim 100$ s at the glass transition temperatures of $T_g \sim 180$ K–210 K reported for hydrated globular proteins. However, this relation is clearly violated for hydrated elastin, which shows a slow process with essentially the same correlation times $\tau$, see Fig. 9, but a significantly higher glass transition temperature of $T_g \sim 320$ K,[20,24] casting serious doubts on the conjecture to assign the slow process to the $\alpha$ relaxation of hydrated proteins. Further strong evidence against this assignment comes from a series of $^2$H NMR studies,[25,26,28] which observed that the $^2$H spin-lattice relaxation of non-methyl protein deuterons is nonexponential up to ambient temperatures. This finding, which is common to myoglobin,[26] C-phycocyanin,[28] and elastin,[25] indicates nonergodic behavior of these proteins at a time scale of ~1 s. This nonergodicity is incompatible with the identification of the slow process with the $\alpha$ relaxation since, if this were true, the slow/$\alpha$ relaxation would restore ergodicity at its much shorter time scales, e.g., $\tau \sim 1$ ms near 250 K. In view of these shortcomings, we reject the conjecture to attribute the slow process to the $\alpha$ relaxation of protein–water systems.

Rather, we propose that the slow BDS process and the related DSC features can be assigned to a hydration-affected $\beta$ relaxation common to globular and fibrous proteins. This assignment naturally explains that the temperature dependence of the slow BDS process deviates, if at all, only mildly from the Arrhenius behavior and that the DSC signatures are weak and broad.[13–16] In this scenario, the onset of enhanced mean square displacements $u^2(T)$ at ~200 K of hydrated proteins is due to a secondary glass transition at $T_{g,\beta}$, as was conjectured for dry proteins.[63] Hence, we rationalize findings for dry and hydrated proteins on common grounds. Consistently, we see in Fig. 9 that, for both global and fibrous proteins, the $u^2(T)$ crossover occurs when the correlation time of the slow process amounts to $\tau \sim 100$ s. Furthermore, we conjecture that another $u^2(T)$ crossover occurs at the regular glass transition at $T_g \equiv T_{g,\alpha}$ of the hydration-affected $\alpha$ relaxation of the protein. As discussed above, this occurs at $T_3 \approx T_g \sim 320$ K for hydrated elastin. However, it remains a challenging problem for future work to determine whether all proteins show an $\alpha$ relaxation. One may speculate that the $\alpha$ relaxation occurs for largely disordered proteins, such as elastin, resembling segmental motion of polymer melts, while it is largely suppressed for highly ordered proteins, including myoglobin and lysozyme.

Several findings indicated that the dynamical process, which sets in at ~195 K, can be described as a coupled protein–water motion, consistent with conclusions in previous studies on various hydrated proteins.[7,38,42,43,58] Nevertheless, our analysis provided only limited insights into the motional mechanism. More detailed information was available in simulation studies.[28,51,58,69,70,88] For hydrated myoglobin, lysozyme, and elastin-mimetic polypeptide $(VPGVG)_{50}$, computational works reported that correlation functions of translational and rotational backbone dynamics decrease in a power-law-like fashion in the picosecond to nanosecond range.[28,69,70,88] When the temperature is increased, the (negative) slope of the decays grows, resembling the situation for the nearly constant loss associated with cage rattling motions of glass-forming systems.[11,49,64] Moreover, simulation work showed that these power-law decays associated with protein backbone dynamics crucially depend on the mobility of hydration water.[70] Considering these findings, we argue that this power-law-like relaxation is related to the present results above ~195 K. Detailed analysis of simulated trajectories for elastin-like[28,69,70] and other[51,58] proteins revealed that the underlying dynamics involves coupled single-well diffusion of large protein parts and collective correlated forward–backward jumps of neighboring amino acids. Accordingly, the power-law behavior was described by a fractional Ornstein–Uhlenbeck process, a disordered energy landscape model, or a higher-order mode coupling singularity.[69,88] Moreover, it was proposed that the main effect of hydration is to widen the local cages and, thus, to increase the amplitude of localized rattling motions.[58] Consistently, $^2$H NMR work on dry and hydrated perdeuterated C-phycocyanin showed that the protein backbone exhibits exclusively small-angle reorientation up to

temperatures of ~260 K and time scales of ~1 s and that the main consequence of hydration is a mild increase in the amplitude of this motion, where the effect sets in somewhat below 200 K and increases with increasing temperature.[28]

Our results for hydrated elastin do not yield evidence for any $u^2(T)$ break in the temperature range 195 K–320 K, where previous studies on other proteins reported the PDT. Several researchers argued that the PDT occurs when hydration water dynamics enters the experimental time window.[6,31,49] Therefore, we indicate the time scales $\tau_{exp}$ of the used neutron scattering spectrometers in Fig. 9. We see that the temperature dependence of the mean square displacement is stronger for the other proteins than for elastin around 240 K. One may speculate that this finding indicates that elastin has a relatively low resilience due to a large ratio of amino acids without side chains, such as glycine or proline, which were previously described as more rigid.[73] In the chosen representation $u^2$ vs $1/T$, a prominent kink at $T_d \sim 230$ K–250 K is, however, not even clearly observed for the globular proteins. Moreover, it is unexpected that, after scaling to common low-temperature behavior, both datasets for bovine serum albumin agree although the used spectrometer resolutions differ by two orders of magnitude.

Altogether, we propose that the present neutron scattering results for hydrated elastin can be attributed to changes in protein cage rattling motions when crossing a secondary glass transition at $T_2 \equiv T_{g,\beta} \sim 195$ K and the regular glass transition at $T_3 \equiv T_{g,\alpha} \sim 320$ K. Both crossovers result in enhanced mean square displacements $u^2(T)$ of hydrated elastin with respect to dry elastin, which we expect to be independent of spectrometer resolution. The enhanced protein cage rattling motion is coupled to hydration water diffusion. It is related to both the H1 and H2 contributions to the IFW intensity, and hence, the necessity to use two contributions reflects a change in the amplitude of the motion rather than the onset of a different relaxation mode at ~320 K. On the other hand, we find no evidence for any $u^2(T)$ crossover in the temperature range 195 K–320 K, where hydration water dynamics enters the experimental time window and the PDT of other hydrated proteins was detected. This finding is puzzling because water dynamics in the hydration shells of various proteins, including elastin, is very similar, at least with respect to its rotational component. Therefore, it deserves further attention in the future work whether there are still some differences, e.g., regarding to the translational aspect of water motion, which is considered to be of particular relevance to facilitate protein backbone dynamics. Moreover, it may be worthwhile to determine in future neutron scattering work whether the observed crossover temperatures $T_2 \equiv T_{g,\beta} \sim 195$ K and $T_3 \equiv T_{g,\alpha} \sim 320$ K of hydrated elastin are independent of the spectrometer resolution, as expected for the proposed scenario.

## V. CONCLUSIONS

Quasielastic neutron scattering proved useful to gain valuable insights into the dynamical behavior of hydrated elastin over a very broad temperature range. A detailed comparison of findings for dry and hydrated elastin samples allowed us to resolve elastin and water dynamics and to ascertain their couplings. Furthermore, analyses of both elastic and quasielastic contributions to the dynamic structure factor in fixed frequency windows provided access to mean square displacements and distributions of correlation times or diffusion coefficients. Finally, exploiting that elastin differs from previously studied proteins with respect to a much higher glass transition temperature $T_g$, while water dynamics are similar in the hydration shells of various proteins, it was possible to scrutinize current models of protein–water couplings.

We found that methyl group rotation is very similar in dry and hydrated elastin and dominates the experimental results particularly at low temperatures. It is well described by a Gaussian distribution of activation energies $G(E)$ characterized by a mean value of $E_m = 0.17$ eV and a standard deviation of $\sigma = 0.04$ eV. Based on these results, it was possible to remove methyl group contributions and to unravel a coupled elastin–water motion, which is strongly heterogeneous and sets in at ~195 K. The involved water motion is of a diffusive nature. It is described by a Gaussian distribution of activation energies with $E_m = 0.57$ eV and $\sigma = 0.08$ eV. This Arrhenius behavior of water diffusion is in agreement with previous results for water reorientation, indicating that translational and rotational motions of elastin hydration water are governed by a common energy landscape. However, it is at variance with a fragile-to-strong crossover reported for protein hydration waters at ~225 K. The water-related elastin motion is localized. Based on a detailed comparison with literature data, in particular, simulation results, we conclude that it can be attributed to backbone cage rattling motion related to the nearly constant loss phenomenon. Moreover, we argue that its onset near ~195 K is related to a secondary glass transition, which occurs when the $\beta$ relaxation of the protein has a correlation time of $\tau_\beta \sim 100$ s, while a crossover in its temperature dependence is due to changes in the temperature dependence of the amplitude of cage rattling motion when crossing the regular glass transition $T_g = 320$ K of hydrated elastin, where the $\alpha$ relaxation of the protein obeys $\tau_\alpha \sim 100$ s. On the other hand, we did not observe a crossover in the temperature-dependent displacements of elastin atoms when water dynamics enters the time window of the scattering experiment near 240 K.

## SUPPLEMENTARY MATERIAL

See the supplementary material for details on the determination of mean square displacements from the $q$ dependence of the elastic intensity and for mean square displacements obtained for elastin with a hydration level of $h = 0.4$ g/g.

## ACKNOWLEDGMENTS

The authors gratefully acknowledge the financial support provided by JCNS to perform the neutron scattering measurements at the Heinz Maier-Leibnitz Zentrum, Garching, Germany. Moreover, financial support from the Deutsche Forschungsgemeinschaft (DFG) in the framework of FOR 1583 through Project No. Vo-905/8-2 is gratefully acknowledged.

## DATA AVAILABILITY

The data that support the findings of this study are available from the corresponding author upon reasonable request.

## REFERENCES


[1] B. Bagchi, Chem. Rev. **105**, 3197 (2005).
[2] Y. Levy and J. N. Onuchic, Annu. Rev. Biophys. Biomol. Struct. **35**, 389 (2006).
[3] P. W. Fenimore, H. Frauenfelder, S. Magazù, B. H. McMahon, F. Mezei, F. Migliardo, R. D. Young, and I. Stroe, Chem. Phys. **424**, 2 (2013).
[4] S. Khodadadi and A. P. Sokolov, Soft Matter **11**, 4984 (2015).
[5] M.-C. Bellissent-Funel, A. Hassanali, M. Havenith, R. Henchman, P. Pohl, F. Sterpone, D. van der Spoel, Y. Xu, and A. E. Garcia, Chem. Rev. **116**, 7673 (2016).
[6] H. Frauenfelder, G. Chen, J. Berendzen, P. W. Fenimore, H. Jansson, B. H. McMahon, I. R. Stroe, J. Swenson, and R. D. Young, Proc. Natl. Acad. Sci. U. S. A. **106**, 5129 (2009).
[7] W. Doster, Eur. Biophys. J. **37**, 591 (2008).
[8] S. Khodadadi, J. H. Roh, A. Kisliuk, E. Mamontov, M. Tyagi, S. A. Woodson, R. M. Briber, and A. P. Sokolov, Biophys. J. **98**, 1321 (2010).
[9] M. Rosenstihl, K. Kämpf, F. Klameth, M. Sattig, and M. Vogel, J. Non-Cryst. Solids **407**, 449 (2015).
[10] S. Cerveny, F. Mallamace, J. Swenson, M. Vogel, and L. Xu, Chem. Rev. **116**, 7608 (2016).
[11] K. L. Ngai, S. Capaccioli, and A. Paciaroni, Biochim. Biophys. Acta - Gen. Subj. **1861**, 3553 (2017).
[12] S. Capaccioli, K. L. Ngai, S. Ancherbak, M. Bertoldo, G. Ciampalini, M. S. Thayyil, and L.-M. Wang, J. Chem. Phys. **151**, 034504 (2019).
[13] H. Jansson and J. Swenson, Biochim. Biophys. Acta - Proteins Proteomics **1804**, 20 (2010).
[14] A. Panagopoulou, A. Kyritsis, R. Sabater i Serra, J. L. Gómez Ribelles, N. Shinyashiki, and P. Pissis, Biochim. Biophys. Acta - Proteins Proteomics **1814**, 1984 (2011).
[15] A. Panagopoulou, A. Kyritsis, N. Shinyashiki, and P. Pissis, J. Phys. Chem. B **116**, 4593 (2012).
[16] M. Nakanishi and A. P. Sokolov, J. Non-Cryst. Solids **407**, 478 (2015).
[17] M. Fomina, G. Schirò, and A. Cupane, Biophys. Chem. **185**, 25 (2014).
[18] K. Sasaki, I. Popov, and Y. Feldman, J. Chem. Phys. **150**, 204504 (2019).
[19] V. Samouillan, J. Dandurand, C. Lacabanne, and W. Hornebeck, Biomacromolecules **3**, 531 (2002).
[20] V. Samouillan, C. André, J. Dandurand, and C. Lacabanne, Biomacromolecules **5**, 958 (2004).
[21] V. Samouillan, D. Tintar, and C. Lacabanne, Chem. Phys. **385**, 19 (2011).
[22] C. Gainaru, A. Fillmer, and R. Böhmer, J. Phys. Chem. B **113**, 12628 (2009).
[23] S. A. Lusceac, M. Rosenstihl, M. Vogel, C. Gainaru, A. Fillmer, and R. Böhmer, J. Non-Cryst. Solids **357**, 655 (2011).
[24] A. Panagopoulou, A. Kyritsis, M. Vodina, and P. Pissis, Biochim. Biophys. Acta - Proteins Proteomics **1834**, 977 (2013).
[25] M. Vogel, Phys. Rev. Lett. **101**, 225701 (2008).
[26] S. A. Lusceac, M. R. Vogel, and C. R. Herbers, Biochim. Biophys. Acta - Proteins Proteomics **1804**, 41 (2010).
[27] A. Perry, M. P. Stypa, B. K. Tenn, and K. K. Kumashiro, Biophys. J. **82**, 1086 (2002).
[28] K. Kämpf, B. Kremmling, and M. Vogel, Phys. Rev. E **89**, 032710 (2014).
[29] A. L. Lee and A. J. Wand, Nature **411**, 501 (2001).
[30] W. Doster, S. Cusack, and W. Petry, Nature **337**, 754 (1989).
[31] W. Doster, Biochim. Biophys. Acta - Proteins Proteomics **1804**, 3 (2010).
[32] W. Doster, S. Busch, A. M. Gaspar, M. S. Appavou, J. Wuttke, and H. Scheer, Phys. Rev. Lett. **104**, 098101 (2010).
[33] W. Doster, J. Non-Cryst. Solids **357**, 622 (2011).
[34] W. Doster, H. Nakagawa, and M. S. Appavou, J. Chem. Phys. **139**, 045105 (2013).
[35] A. M. Tsai, D. A. Neumann, and L. N. Bell, Biophys. J. **79**, 2728 (2000).
[36] G. Zaccai, Science **288**, 1604 (2000).
[37] K. Wood, M. Plazanet, F. Gabel, B. Kessler, D. Oesterhelt, D. J. Tobias, G. Zaccai, and M. Weik, Proc. Natl. Acad. Sci. U. S. A. **104**, 18049 (2007).
[38] K. Wood, A. Frölich, A. Paciaroni, M. Moulin, M. Härtlein, G. Zaccai, D. J. Tobias, and M. Weik, J. Am. Chem. Soc. **130**, 4586 (2008).
[39] J. H. Roh, V. N. Novikov, R. B. Gregory, J. E. Curtis, Z. Chowdhuri, and A. P. Sokolov, Phys. Rev. Lett. **95**, 038101 (2005).
[40] J. H. Roh, J. E. Curtis, S. Azzam, V. N. Novikov, I. Peral, Z. Chowdhuri, R. B. Gregory, and A. P. Sokolov, Biophys. J. **91**, 2573 (2006).
[41] G. Caliskan, R. M. Briber, D. Thirumalai, V. Garcia-Sakai, S. A. Woodson, and A. P. Sokolov, J. Am. Chem. Soc. **128**, 32 (2006).
[42] S. Khodadadi, S. Pawlus, J. H. Roh, V. Garcia Sakai, E. Mamontov, and A. P. Sokolov, J. Chem. Phys. **128**, 195106 (2008).
[43] S. Khodadadi and A. P. Sokolov, Biochim. Biophys. Acta - Gen. Subj. **1861**, 3546 (2017).
[44] J. D. Nickels, H. O'Neill, L. Hong, M. Tyagi, G. Ehlers, K. L. Weiss, Q. Zhang, Z. Yi, E. Mamontov, J. C. Smith, and A. P. Sokolov, Biophys. J. **103**, 1566 (2012).
[45] S.-H. Chen, L. Liu, E. Fratini, P. Baglioni, A. Faraone, and E. Mamontov, Proc. Natl. Acad. Sci. U. S. A. **103**, 9012 (2006).
[46] E. Cornicchi, M. Marconi, G. Onori, and A. Paciaroni, Biophys. J. **91**, 289 (2006).
[47] S. Magazu, F. Migliardo, and A. Benedetto, J. Phys. Chem. B **115**, 7736 (2011).
[48] G. Schiró, F. Natali, and A. Cupane, Phys. Rev. Lett. **109**, 128102 (2012).
[49] S. Capaccioli, K. L. Ngai, S. Ancherbak, and A. Paciaroni, J. Phys. Chem. B **116**, 1745 (2012).
[50] G. Schiro, Y. Fichou, F.-X. Gallat, K. Wood, F. Gabel, M. Moulin, M. Härtlein, M. Heyden, J.-P. Colletier, A. Orecchini, A. Paciaroni, J. Wuttke, D. J. Tobias, and M. Weik, Nat. Commun. **6**, 6490 (2015).
[51] Z. Liu, J. Huang, M. Tyagi, H. O'Neill, Q. Zhang, E. Mamontov, N. Jain, Y. Wang, J. Zhang, J. C. Smith, and L. Hong, Phys. Rev. Lett. **119**, 048101 (2017).
[52] G. Schirò, C. Caronna, F. Natali, M. M. Koza, and A. Cupane, J. Phys. Chem. Lett. **2**, 2275 (2011).
[53] Z. Yi, Y. Miao, J. Baudry, N. Jain, and J. C. Smith, J. Chem. Phys. B **116**, 5028 (2012).
[54] M. Trovaslet, M. Trapp, M. Weik, F. Nachon, P. Masson, M. Tehei, and J. Peters, Chem. Biol. Interact. **203**, 14 (2013).
[55] J. Peters, N. Martinez, M. Trovaslet, K. Scannapieco, M. M. Koza, P. Masson, and F. Nachon, Phys. Chem. Chem. Phys. **18**, 12992 (2016).
[56] D. Zeller, P. Tan, L. Hong, D. D. Bari, V. G. Sakai, and J. Peters, Phys. Rev. E **101**, 032415 (2020).
[57] G. Zaccai, Biochim. Biophys. Acta - Gen. Subj. **1864**, 129475 (2020).
[58] L. Hong, X. Cheng, D. C. Glass, and J. C. Smith, Phys. Rev. Lett. **108**, 238102 (2012).
[59] F. Parak, E. W. Knapp, and D. Kucheida, J. Mol. Biol. **161**, 177 (1982).
[60] B. F. Rasmussen, A. M. Stock, D. Ringe, and G. A. Petsko, Nature **357**, 423 (1992).
[61] M. Tarek and D. J. Tobias, Phys. Rev. Lett. **88**, 138101 (2002).
[62] M. Krishnan, V. Kurkal-Siebert, and J. C. Smith, J. Phys. Chem. B **112**, 5522 (2008).
[63] K. L. Ngai, L. Hong, S. Capaccioli, and A. Paciaroni, J. Mol. Liq. **286**, 110810 (2019).
[64] K. L. Ngai, S. Capaccioli, and A. Paciaroni, J. Chem. Phys. **138**, 235102 (2013).
[65] M. Trapp, M. Trovaslet, F. Nachon, M. M. Koza, L. van Eijck, F. Hill, M. Weik, P. Masson, M. Tehei, and J. Peters, J. Chem. Phys. B **116**, 14744 (2012).
[66] K. L. Ngai, J. Non-Cryst. Solids **275**, 7 (2000).
[67] P. Kumar, Z. Yan, L. Xu, M. G. Mazza, S. V. Buldyrev, S.-H. Chen, S. Sastry, and H. E. Stanley, Phys. Rev. Lett. **97**, 177802 (2006).
[68] A. Panagopoulou, A. Kyritsis, A.-M. Aravantinou, D. Nanopoulos, R. S. i Serra, J. L. Gómez Ribelles, N. Shinyashiki, and P. Pissis, Food Biophys. **6**, 199 (2011).
[69] K. Kämpf, F. Klameth, and M. Vogel, J. Chem. Phys. **137**, 205105 (2012).
[70] J. Geske, M. Harrach, L. Heckmann, R. Horstmann, F. Klameth, N. Müller, E. Pafong, T. Wohlfromm, B. Drossel, and M. Vogel, Z. Phys. Chem. **232**, 1187 (2018).
[71] B. Frick, J. Combet, and L. van Eijck, Nucl. Instrum. Methods Phys. Res., Sect. A **669**, 7 (2012).
[72] M. T. F. Telling, L. Clifton, J. Combet, B. Frick, S. Howells, and V. G. Sakai, Soft Matter **8**, 9529 (2012).
[73] G. Schiró, C. Caronna, F. Natali, and A. Cupane, J. Am. Chem. Soc. **132**, 1371 (2010).

[74]O. Russina, A. Triolo, Y. Aihara, M. T. F. Telling, and H. Grimm, Macromolecules **37**, 8653 (2004).
[75]K. Raju and R. A. Anwar, J. Biol. Chem. **262**, 5755 (1987).
[76]J. Wuttke, A. Budwig, M. Drochner, H. Kämmerling, F.-J. Kayser, H. Kleines, V. Ossovyi, L. C. Pardo, M. Prager, D. Richter, G. J. Schneider, H. Schneider, and S. Staringer, Rev. Sci. Instrum. **83**, 075109 (2012).
[77]H. Maier-Leibnitz Zentrum *et al.*, J. Large Scale Res. Facil. JLSRF **1**, A30 (2015).
[78]M. Bée, *Quasielastic Neutron Scattering: Principles and Applications in Solid-State Chemistry, Biology and Materials Science* (Adam Hilger, Bristol, 1988).
[79]A. Heuer, J. Phys.: Condens. Matter **20**, 373101 (2008).
[80]R. Böhmer, G. Diezemann, G. Hinze, and E. Rössler, Prog. Nucl. Magn. Reson. Spectrosc. **39**, 191 (2001).
[81]M. Vogel, P. Medick, and E. A. Rössler, Annu. Rep. NMR Spectrosc. **56**, 231 (2005).
[82]U. Buchenau and R. Zorn, Europhys. Lett. **18**, 523 (1992).
[83]H.-H. Grapengeter, B. Alefeld, and R. Kosfeld, Colloid Polym. Sci. **265**, 226 (1987).
[84]M. Rosenstihl and M. Vogel, J. Chem. Phys. **135**, 164503 (2011).
[85]D. W. Urry, T. Hugel, M. Seitz, H. E. Gaub, L. Sheiba, J. Dea, J. Xu, and T. Parker, Philos. Trans. R. Soc. London, Ser. B. **357**, 169 (2002).
[86]M. Baer, E. Schreiner, A. Kohlmeyer, R. Rousseau, and D. Marx, J. Phys. Chem. B **110**, 3576 (2006).
[87]M. T. Cicerone and M. Tyagi, J. Chem. Phys. **146**, 054502 (2017).
[88]M. Lagi, P. Baglioni, and S. H. Chen, Phys. Rev. Lett. **103**, 108102 (2009).